Fuel Processing Technology (2015). 131, 338-347.
DOI: http://dx.doi.org/10.1016/j.fuproc.2014.11.036

DEFLUIDIZATION AND AGGLOMERATION OF A FLUIDIZED BED REACTOR DURING *CYNARA CARDUNCULUS* L. GASIFICATION USING SEPIOLITE AS BED MATERIAL

D. Serrano[a]*, S. Sánchez-Delgado[a], C. Sobrino[a], C. Marugán-Cruz[a]

[a]*Carlos III University of Madrid, Thermal and Fluid Engineering Department. Avda. de la Universidad 30, 28911 Leganés (Madrid), Spain*

*T: +34916248884; E-mail: daserran@ing.uc3m.es

Abstract

This work studies the defluidization time and the agglomerates generation in a Bubbling Fluidized Bed (BFB) reactor during *Cynara Cardunculus* L. gasification using, separately, two different bed materials, silica sand and sepiolite ($Mg_8Si_{12}O_{30}(OH)_4(OH_2)_48H_2$). The high adsorption capacity and the elemental composition of the sepiolite make it suitable as an alternative bed material in order to reduce agglomeration. Experiments were performed on a stainless steel lab-scale BFB reactor operating with air as gasifying agent at different air excess ratios (u/u_{mf}). A quartz reactor was alternatively used for the visualization of bed material and biomass during gasification, allowing to observe the agglomerate formation process. Pressure signals were analyzed both in time and frequency domain to determine the defluidization time. Furthermore, the shape and size of the bed material after the experiments were evaluated. Higher defluidization times in the case of sepiolite were measured. Particle sizes were affected by the type of bed material and the air excess and agglomerates of different shapes were formed for sepiolite and silica sand.

Keywords

Biomass; gasification; fluidized bed; sepiolite; agglomeration; defluidization

1. Introduction

Biomass conversion into a useful energy resource is done by several thermochemical methods (pyrolysis, gasification and combustion) depending on the oxygen provided to the processes to produce heat, electricity, chemicals or engine fuels [1]. Biomass gasification is a promising technology as an alternative to fossil fuels and to reduce greenhouse emissions [2]. It consists

on a substoichiometric oxidizing conditions process at high temperature in order to obtain a combustible gas (H_2, CO, CH_4, N_2, CO_2 and light hydrocarbons) which can be burned in boilers or gas engines [3].

The typical reactor types employed in gasification are fixed-bed and fluidized-bed reactors [4]. Fluidized-bed (FB) gasifiers have several advantages over fixed-bed reactors like uniform temperature distribution, better temperature control, good gas-solids mixing, better heat and mass transfer rates or wide variety of feedstock quality and size distribution [5,6]. However, this technology also has some disadvantages like bed agglomeration, leading into hot zones, thermal stresses on measurement equipment, defluidization and unscheduled shut downs of the reactor.

The knowledge of the biomass composition, the use of alternative bed materials or the variation of the operating conditions are different ways to prevent the agglomeration within FB, avoiding the FB defluidization. Several authors have studied the influence of these parameters in the defluidization process. Bartels et al. [7] and Khan et al. [8] reviewed different strategies aimed to alleviate agglomeration in fluidized beds. Some of these strategies try to define operational actions that reduce agglomeration or avoid the bed defluidization, such as fuel pre-treatment or co-feeding an additional fuel. In this sense, Lin et al. [9] studied the influence of different parameters such as temperature or the particle size on the agglomeration process during wheat straw combustion. Liliedhal et al. [10] investigated the effect of different parameters on the agglomeration behavior of biomass gasifier and proposed an empirical expression to determine the maximum temperature at which the fluidization is stable as a function of pressure, ash composition, bed material and gasifying agent. Sevonious et al. [11] used three different pure potassium salts in a FB of quartz sand in order to understand the role of the separate components of the biomass in the agglomeration mechanisms.

As stated above, other strategies to prevent this undesirable problem are concern with the use of additives or the utilization of different bed materials as an alternative to silica sand [12]. Catalysts like dolomite, olivine, magnesite or alumina are widely used in biomass gasification,

as bed materials, to improve product gas quality and to reduce the tar content in the flue gas. Besides, these materials can also serve as agglomeration inhibitors and extent the fluidization state. According to Bartels et al. [7], bed materials low in or free of silica sand are chosen to avoid the tendency of silica to form low-melting point silicates with alkali salts which cause agglomeration. Fryda et al. [13] employed olivine, obtaining higher defluidization temperatures due to its Fe and Mg content and a particle distribution moved towards bigger diameters than fresh bed material. Liliedhal et al. [10] reported the use of magnesite, dolomite and olivine as bed materials which improved agglomeration. Siedlecki and de Jong [14] and Xue et al. [3] also used magnesite as bed material enhancing the agglomeration behavior.

Sepiolite ($Mg_8Si_{12}O_{30}(OH)_4(OH_2)_48H_2$) is a low density and high porosity clay mineral that can be employed as an alternative bed material and, to our knowledge, it has not been used in FB combustors or gasifiers before. Sepiolite is mainly composed of silice (58-59 wt% as oxide) and magnesium (24-25 wt% as oxide) [15]. Spain is the largest producer of sepiolite and accounted for about 95% of the world's annual production in the last decade [16].

A considerable amount of work has been dedicated to developing methods for the detection of agglomeration or defluidization of FB reactors. Most of the methods proposed are concerned with the measurement of a process variable (pressure and/or temperature) [7]. The measurement of the average pressure drop across a vertical section of the bed, which is a common practice in industry, can be used to detect the occurrence of defluidization, but not the shift towards defluidization, as this variable is rather insensitive to changes in the superficial gas velocity [17]. The measurement of the standard deviation or the variance of differential or absolute pressure fluctuations has been shown to be a successful way to detect agglomeration. Scala and Chirone [18,19] used the variance of the pressure measured at the middle section of the bed, sampled with piezoresistive pressure transducers at 100 Hz, to detect the defluidization onset during the combustion of pine seed shells in a bench-scale and in a pilot-scale reactor. Similarly, van Ommen et al. [17] proposed the monitorization of the standard deviation of absolute pressure fluctuations to detect defluidization. In this method the selection of a threshold value

under which the standard deviation has to decrease to consider that a defluidization event is forthcoming is a choice between detection speed on the one hand and risk of false alarms in the other hand. Frequency domain methods, as the transient power spectral density, have also been proposed as a defluidization detection technique [20]. In this method the signal is divided into a number of segments and the power spectral density is calculated for each of them, resulting in a set of spectral densities as a function of time. Then, the defluidization onset is detected by the dominant frequency disappearance.

On the other hand, the measurement of temperature can be also used to detect agglomeration. Among the differences options in the literature, the evaluation of the difference between the instantaneous temperatures measured by two thermocouples placed at a certain vertical distance apart [18,19], which value increases due to agglomeration, seems to be quite sensitive to the shift toward defluidization.

Different plants like miscanthus or cardoon are being investigated as a resource for biomass gasification [3,21]. A cardoon that can serve as an alternative to biomass production in lands that are not employed for food purposes is *Cynara Cardunculus* L. [22]. This thistle is a perennial plant which is native to Mediterranean regions but also grows as a weed in some parts of the world like Argentina or California [23]. This kind of climate is characterized by hot and dry summers what makes it suitable for *Cynara* adaptation [22,23]. Grammelis et al. [24] reported some advantages in the cultivation of this energy crop like a decrease in nitrogen pollution, reduction of agro-chemicals, low water irrigation and improvement of solid characteristics, being also the cheapest biofuel in comparison with other energy crops. Different studies based on the cultivation of this specie [22,24–27] have been carried out due to its importance for biomass production. In Spain, the energy use of Cynara has been investigated under the CARDENER-CM project. However, little literature was published regarding *Cynara Cardunculus* L. gasification. Encinar et al. [28] studied the pyrolysis of *Cynara* in order to determine the quality of the charcoal formed and identify and quantify the gases produced. They also performed steam gasification studies [29], obtaining higher H_2 yield in the case of steam

gasification than pyrolysis under the same temperature. Recently, Abelha et al. [21] reported results on *Cynara* combustion, gasification, co-combustion and co-gasification with *Eucalyptus globules*. The addition of eucalyptus reduced the agglomeration formation caused by the high alkali content of *Cynara* in the combustion and gasification experiments while agglomeration during combustion was completely avoided if a dolomite catalyst was added to the silica sand FB. Christodoulou et al. [30] studied the agglomeration problem during *Cynara* gasification. They concluded that the use of this biofuel is not suitable for long operation periods in large FBs due to its high content of potassium, silica and calcium which lead to the agglomeration and defluidization of the bed, and they proposed the use of another type of biomass to blend with cardoon in order to reduce agglomeration.

The aim of this work is to study the performance of an alternative bed material, sepiolite, in comparison with silica sand which is usually employed in biomass gasifiers in order to study the dynamic behavior of the reactor by means of defluidization time. For this purpose, defluidization time, bed material particle size distribution and agglomerations formed during the gasification of *Cynara Cardunculus* L. were studied. The use of the sepiolite can help to reduce the defluidization of the bed when this cardoon is gasified.

2. Experimental setup

2.1. Biomass and bed materials analysis

Cynara Cardunculus L. was employed as biomass feedstock. A thermogravimetric analyzer was used for proximate analysis. Ultimate analysis was carried out using a CHN elemental analyzer. High heating value (HHV) was also measured by means of an isoperibolic calorimeter oxygen combustion. Finally, inorganic elemental composition analysis using ICP was performed on the fuel. All analyses were accomplished according the corresponding standard for solid biofuels. The results of the *Cynara* characterization are shown in Table 1.

Table 1. *Cynara Cardunculus* L. analysis.

Proximate Analysis		Ultimate Analysis	
Moisture [wt % db]	7.56	Carbon [wt % db]	48.50

Volatile Matter [wt % db]	77.79	Hydrogen [wt % db]	5.52
Fixed Carbon [wt % db]	8.55	Nitrogen[wt % db]	0.80
Ash [wt % db]	6.10	Oxygen[a] [wt % db]	45.18
Ash analysis [g/kg fuel as received]			
Na	6.00	K	8.70
Ca	9.20	Mg	2.10
Al	0.70	Fe	0.60
Si	0.03		
Trace metals [μg/g fuel as received]			
Hg	0.011	As	0.29
Cd	0.10	Se	0.05
Cu	4.42		
High heating value [MJ/kg db]	17.80		

[a] By difference

Biomass was disposed in cylindrical pellets of approximately 6 mm of diameter and 15 mm of length, with a mass distribution centered in 0.4975 g and with a standard deviation of 0.0478 g. Biomass was manually fed into the reactor by its upper part.

Two solids were used as bed material: silica sand and sepiolite (clay). Silica sand has been widely used in FB gasification because it is a cheap and abundant material [31]. However, as stated above, if the biomass has high alkali content it can react with silica particles leading to a partial or complete agglomeration of the bed. In order to avoid this problem, due to the high alkali content of *Cynara* (Table 1), a new bed material, sepiolite, was tested and proposed as an alternative to silica sand. This clay material is a hydrated magnesium phyllosilicate with an empirical formula of $Mg_8Si_{12}O_{30}(OH)_4(OH_2)_4 8H_2$ [32]. It is usually employed in a wide variety of industries as industrial adsorbent, cosmetics, filtering, ceramics or paint due to its adsorbent properties, chemical and mechanical stability and high surface area (~300 m^2/g) [32–34].

The two bed materials were sieved to have a particle diameter between 425 and 600 μm in order to neglect the particle size influence. According to particle size and density, silica sand and sepiolite belongs to type B according to Geldart's classification [35]. Table 2 shows the main bed material properties.

Table 2. Bed material properties.

	Silica sand	Sepiolite
Density [kg/m3]	2645	1551
Void fraction [-]	0.44	0.64
Particle diameter [μm]	425-600	
Minimum fluidization velocity at 850 ºC [m/s]	0.089	0.057

2.2. Experimental facility

All the experiments were executed on a lab-scale Bubbling Fluidized Bed (BFB) operated with air as gasifying agent. The reactor is made of stainless steel 304 with an inner diameter of 52.8 mm. It is divided in two sections: a lower part or plenum where the gasifying agent is preheated, and an upper part where the bed is located (Fig. 1). These two sections have a total length of 570 mm and 910 mm, respectively. A 2 mm thickness perforate plate with 38 holes of 0.5 inner diameter distributed in triangular pitch is enclosed by the plenum and the bed. The plenum is filled with steel wool to increase the residence time of the gasifying agent in this part of the reactor for a better preheating of the gasifying agent before it enters the bed. The whole reactor is surrounded by two electrical furnaces, one for the lower part and another one for the upper part, to provide the energy necessary to get the desired temperature inside the bed and to simulate adiabatic conditions. At the top of the reactor a mirror is located to see inside the gasifier.

Fig 1. Experimental facility.

Two absolute pressure sensors, Honeywell SPT series, and two piezoelectric pressure sensors, Kistler type 7261, were used to measure pressure fluctuations. The signals were collected using a National Instruments data acquisition system type 9234 with 4 analog input channels, 24 bit-resolution, working at a sampling frequency of 400 Hz. Pressure transducers were located in the plenum and in the bed, 30 mm below (P1 and K1) and above (P2 and K2) the distributor plate. Temperature was measured using K-type thermocouples at the same heights as pressure sensors (T1 and T2) and also at 60 mm (T3) and 450 mm (T4) above the distributor as (see Fig. 1).

A quartz reactor with similar characteristics to the previous reactor was also employed to qualitatively observe the bed under certain experimental conditions. A 25 fps video was recorded through a slit in the furnace with a Nikon D5100 camera.

2.3. Experimental procedure

Prior to experiments, the distributor was characterized. Pressure drop through this element ($\Delta P_{dist} = 60440 \cdot u_g^2$ at 850 ºC) was high enough to ensure that the bed and the air supply system were not coupled [36].

At the beginning of each experiment an exact amount of bed material (silica sand or sepiolite) was loaded into the reactor in order to get a bed height of 79.2 mm ($h_b/D = 1.5$). Air supply was turned on and bed temperature was raised to 850 ºC using the electrical furnaces. Once the desired temperature was constant minimum fluidization was measure before each experiment (Table 2). After this, the air flow rate was set according with the air excess for each experiment (Table 3). Fuel rate was calculated in agreement with the equivalent ratio (ER) which is defined as the ratio between the air flow rate introduced into the gasifier and the stoichometric air flow needed for the complete combustion of biomass. Typical values of this parameter for gasification conditions are between 0.2 and 0.4 [37]. Depending on the application in which the product gas will be used a different value should be adopted [38]. In this work, ER = 0.3, was set for all experiments. Before starting biomass feeding, pressure and temperature signals were acquired for 300 s as reference conditions for each experiment. Finally, *Cynara Cardunculus* L. was fed into the gasifier at a constant rate, according with the air flow rate and the ER (Table 3). When pressure fluctuations became zero or very close to this value and the bed looked defluidized in the mirror, biomass feeding was stopped while signals were acquired for another 300 s. After this time, the heaters and the air supply were shut down. Later, when the reactor was cooled down, the bed material was sieved to analyze particle size distribution.

Table 3. Operating conditions.

	Silica Sand (u_{mf} = 0.089 m/s)	Sepiolite (u_{mf} = 0.057 m/s)

Air excess ratio, u/u_{mf}	2	4	6	8	10	2	4	6	8	10
Air flow [l/min]	6.38	13.2	19.8	26.5	33.1	4.01	8.09	12.35	14.74	19.60
Fuel rate [g/min]	5.19	10.54	15.43	20.87	25.90	3.38	6.46	9.79	12.24	16.44
ER	0.29	0.30	0.30	0.30	0.30	0.28	0.30	0.30	0.29	0.28
Bed aspect ratio	1.5					1.5				
Bed material [kg]	0.257					0.097				

2.4. Analysis methodology

The analysis of pressure signals was performed using time and frequency domain methods in order to detect defluidization time. They were acquired using the piezoelectric pressure sensors located in the bed.

On the one hand, standard deviation of pressure fluctuation signal was used for time analysis because of the influence of gas velocity on pressure fluctuations. This standard deviation remains in zero or very close to it until the onset of fluidization and, from this point, it increases linearly with gas velocity [39]. For this reason, this first approach has widely used to identify a regime change or defluidization time [20,40]. The standard deviation was calculated for 30 s time periods along the time-series with a 15 s overlapping between periods. Using this result, a threshold can be defined in order to distinguish whether the bed is defluidized or not. Different threshold values were adopted to compare their effect on the value of the defluidization time.

On the other hand, power spectral density (PSD) was calculated for the frequency analysis. The PSD was calculated using Welch's periodogram [41] with a Hanning window [42] for different segments along the signal, obtaining different PSD function of time [40]. As a result, the frequency with the highest energy was chosen as the dominant frequency for each period of time. Finally, these values were plotted as a function of time in order to identify changes in the dominant frequency of the bed, and therefore, on the fluidization regime [20].

Pressure drop across the bed acquired using the absolute pressure sensor (P2) and temperature difference between the two thermocouples inside the bed (T2 and T3) were also measured. Significant changes in the standard deviation and the frequency of the pressure fluctuations

during the defluidization of the bed must agree with a decrease in the pressure drop across the bed and with an increase in the relative temperature difference between two positions in the bed. Visual observation of the surface of the bed was used to confirm the defluidization of the bed.

Once the experiment was finished, bed material was sieved to compare the particle distribution after and before the experiment. Sieves ranging from 2 mm to 250 μm were used for this task. Particles at each sieve were weighted and the mass fraction with respect to the fresh bed material was obtained.

In order to illustrate the different types and sizes of agglomerates, photographs were also taken at the end of the experiments.

3. Results and discussion

3.1. Visual observations

For silica sand experiments, biomass remained on the bed surface and a flame appeared due to the combustion of biomass. As biomass was continuously fed the flame reduced its size but it did not extinguish because of the partial combustion of biomass and volatiles. No char or pellets were observed inside the bed during the experiment. The mixing between biomass and bed material was very poor and all pellets remained on the bed surface. As a consequence, devolatilization and gasification reactions took place in this part of the bed without much interaction with bed material, as it is shown in Fig. 2a and 2b. Contrary to this, a different behavior was observed when sepiolite was used: pellets sank into the bed (see Fig. 2d and 2e) and few and small flames appeared. These flames were very sporadic occurring in three different situations: when the pellet was transported to the surface of the bed, when the pellet was reached by exogenous bubbles which were always present in the bed under aggregative fluidization conditions or when an endogenous bubble of volatiles was formed around the pellet. The formation of endogenous bubbles and their influence on fuel segregation was studied by Fiorentino et al. [43,44]. According to this phenomenon, for the sand experiments, the endogenous bubbles induced segregation of the fuel particle at the top of the bed. This was also

promoted by the high density of the bed material in comparison with the pellet density, making the pellet to float on the top of the bed. On the other hand the pellet sank in the bed of sepiolite due to its low density, while the endogenous and exogenous bubbles transported the pellet and volatile matter to the bed surface. Therefore, these two effects for the sepiolite bed resulted in a better dispersion of the fuel particles that brought about a better dispersion of ash. In sepiolite experiments pellets were seen moving all around the the bed and char devolatilization and conversion occurred inside the whole bed with a higher interaction with the bed material than in the sand case.

Fig 2. Snapshots (using the quartz reactor) obtained during gasification experiments ($u/u_{mf} = 4$): a), b) and c) silica sand; d), e) and f) sepiolite.

The region where ash was generated differed from one bed material to the other. For silica sand this zone was very narrow and it was located at the top of the reactor contrary to sepiolite in which pellet circulation distributed the ash all over the bed. This behavior had strong influence during defluidization. In the first set of experiments, using silica sand, ash accumulation happened to meet a hot zone forming a flat plate agglomerate on the top of the FB. This maldistribution of ash made the bed to defluidized earlier than sepiolite where the hot zone was moving through the bed increasing defluidization time. Fig. 2c and 2f show the moment when the bed was defluidized for both silica sand and sepiolite, respectively. It can be seen how all pellets were located at the top of the bed forming a lid for silica sand while for sepiolite the agglomerate was difficult to see because it was a big cylinder inside the reactor.

3.2. Time analysis

Fig. 3 shows the pressure and temperature signals acquired for the case of $u/u_{mf} = 4$. Fig. 3a and 3d presents the pressure fluctuations measured inside the bed for silica sand and sepiolite. While the bed is fluidized, pressure fluctuations are very different from zero. When defluidization was about to start, a sharp decrease in the pressure fluctuations was observed during a short period of time. After this, it can be seen that the value remains very close to zero. In Fig. 3b and 3e

pressure drop across the bed is shown. As it is well known, pressure drop across the bed remains in a constant value while the bed is fluidized. A reduction from this value can be understood as a change in the fluidization state towards a defluidization regime. In this case, when defluidization appeared, this reduction was seen in the pressure drop across the bed. Finally, Fig. 3c and 3f shows the relative temperature difference measured between T2 and T3, as an indicator of the effectiveness of bed mixing [19]. When defluidization occurred bed mixing was stopped and temperature difference along the bed began to increase. Comparing these figures for each bed material, it can be seen that the defluidization seems to be predicted more or less at the same instant by the different process parameters measured which is also in agreement with visual observations using the mirror placed at the top of the reactor.

Fig. 3. Pressure and temperature signals for silica sand and sepiolite (u/u_{mf}= 4): a) and d) pressure fluctuations inside the bed; b) and e) pressure drop across the bed; c) and f) relative temperature difference between different heights.

For a better determination of the defluidization time and a better comparison of the results, the standard deviation of pressure fluctuations was also calculated (see Fig. 4).

When silica sand was tested (Fig. 4a), the standard deviation remained constant value until defluidization took place. As biomass remained on the top of the bed, no difference was observed between the first part of the signal where only air was passing through the bed and the part of the signal where biomass was continuously fed. The transition between the two regimens (fluidized and defluidized) was very clear and it occurred in a very short period of time. At a low air excess, u/u_{mf}= 2, the standard deviation did not drop to zero although the reactor seemed defluidized. A plausible explanation is that beneath the agglomerate formed on the bed surface, the bed remained fluidized. In fact, no changes in the signal of pressure fluctuations with time were observed for this case.

Fig. 4. Standard deviation of pressure fluctuations inside the bed: a) silica sand and b) sepiolite.

When using the sepiolite as bed material different trends were observed (Fig. 4b). Before biomass feeding, the standard deviation of the pressure signal remained constant. However, once biomass feeding started a rapid increase in the standard deviation was detected. The better mixing of biomass with bed material led to the release of volatiles inside the bed, creating endogenous bubbles in addition to the air bubbles formed at the distributor plate. The more bubbles the higher pressure fluctuations due to a greater probability of bubbles coalescence and therefore, larger bubble diameter [45,46]. For u/u_{mf} = 2, 4 and 6 the standard deviation increased around a 50% from the signal at nominal conditions (before biomass feeding), having the higher production of bubbles an important effect. For u/u_{mf} = 8 this increment was relatively small amd for the case of u/u_{mf} = 10 there was no evidence of this effect, furthermore standard deviation started to decrease. It is well known that beyond a certain value of gas velocity where bubbles reach a maximum size, bubbles break into smaller ones, reducing the amplitude of pressure fluctuations[47]: at this high gas velocities the effect of the appearance of endogenous bubbles does not increase the amplitude of pressure fluctuations because the fluidization is very vigorous already and bubble coalescence is overtaken by bubble splitting [48]. The standard deviation decreased to zero for sepiolite at all the experimental conditions as it can be seen in Fig. 4b, as the agglomerate formed is uniformly distributed over the bed.

3.3. Frequency analysis

The PSD for pressure fluctuations at different time were calculated for silica sand and sepiolite in order to obtain the defluidization time. As it was explained in the analysis methodology section, the PSD was obtained for different segments along the signal and the mayor frequency in each segment was chosen as the dominant frequency. Fig. 5 shows the PSD of pressure fluctuations for one of the experiments (sepiolite, u/u_{mf}=6) at two instants during the experiment, before and after the defluidization of the bed. The dominant frequency for each spectrum is marked in the plot. The evolution of this frequency along the time is showed in Fig. 6. While there was a bubbling fluidized conditions in the bed a dominant frequency appeared

with a constant value. However, when defluidization occurred the frequency sharply decreased to zero.

Fig. 5. PSD of pressure fluctuations for sepiolite (u/u_{mf}=6) at two different instants. At a time of 41 min the bed was fluidized and at a time of 45 min the bed was defluidized. The dominant frequency of each spectrum is marked with a circle in the plot.

During the experiments with silica sand (see Fig. 6a) and at high air excesses (u/u_{mf} = 6, 8 and 10) the frequency recovered its value after defluidization. This transition could make one think that the bed was again fluidized; however, looking at Fig. 4a, it can be seen that the standard deviation remained very close to zero and visual observations using the mirror corroborated that the bed was still defluidized.

Fig. 6. Dominant frequency of the power spectrum of pressure fluctuations inside the bed as a function of time: a) silica sand and b) sepiolite.

3.4. Defluidization time

The defluidization times measured using the two different methods explained above were compared (see Fig. 7). For the standard deviation method, the transition between fluidization and defluidization state could be ambiguous depending on the bed material employed in the experiments. Defluidization was clearly distinguished in silica sand tests; however, this transition was more gradual with sepiolite. Therefore, a threshold must be defined to differentiate fluidization and defluidization when using the standard deviation method. Three different thresholds were proposed: 75%, 50% and 25% of the standard deviation for u/u_{mf} = 2 where fluidization is less intense, and therefore the most restrictive air excess. On the other hand, the PSD method, the defluidization event led to a sharp decrease of the dominant frequency, and hence, the defluidization time is almost insensitive to the threshold value chosen.

Fig. 7 shows the defluidization time obtained using the standard deviation and the PSD method for all the experiments. It can be notice that, in general, the results are quite similar for the three

thresholds defined for the standard deviation method and are also comparable to the values obtained using the PSD method. For $u/u_{mf} = 2$ with silica sand, the 75% threshold predicted a very short defluidization time in comparison with the PSD method and the bed looked fluidized in the mirror at this time. Besides, the standard deviation method did not fall below the 25% threshold during this experiment although the bed looked defluidized in the mirror. As a result, the threshold selected for the standard deviation method which predicts defluidization time in agreement with the PSD method and the visual observation of the bed is the 50% threshold. Therefore, for this type of reactor and using these experimental conditions the reactor can be considered defluidized when the standard deviation of pressure fluctuations falls below 15 Pa and 4 Pa for silica sand and sepiolite respectively.

Fig. 7. Defluidization time: a) silica sand and b) sepiolite.

Comparing both bed materials, it can be noted that a clear improvement in the defluidization time was achieved in the sepiolite experiments. Both chemical and physical properties of the sepiolite can affect this behavior. In order to avoid agglomeration, silica sand should be replaced by another bed material with less silica content to reduce the formation of low-melting silicates [7]. According to this, sepiolite has around a 40 wt% less silica oxide than silica sand. Some of this silica is substituted by magnesium oxide, a common component of other bed materials like magnesite ($MgCO_3$) or dolomite ($CaMg(CO_3)_2$) which improves agglomeration. Alkali earth metals such as Mg or Ca commonly reduces agglomeration [13] although sometimes they can promote it if the ratio Na/Mg or Na/Ca are high [49]. On the other hand, sepiolite presents a large surface area due its high porosity. This property can improve the adsorption of the melt phases formed during the process. Besides, sepiolite density helps to get a better mixing and, therefore, a better distribution of ash inside the bed, avoiding hot zones. All these properties (composition, porosity and density) serve to reduce agglomeration during the gasification of biomass. Nevertheless, sepiolite has some attrition problems when comparing with silica sand. A cold attrition test was performed at ratio u/u_{mf}=10 during 6 hours obtaining mass differences before and after the experiment less than 10%. In terms of particle size distribution, the

differences before and after the attrition test were also less than 10% for each particle range. Therefore, attrition might be considered a minor drawback for sepiolite due to the improvements obtained in terms of operation time when comparing with silica sand. Besides, sepiolite attrition is not as high as in dolomite, although catalytic effects of sepiolite should be also analyzed in order to compare with dolomite.

The effect of the air excess ratio on defluidization time was also different with silica sand and with sepiolite. For the experimental conditions studied and the lab-scale facility an optimum value for the u/u_{mf} ratio was obtained (see Fig. 7). From this value, $u/u_{mf}=6$ and $u/u_{mf}=4$ for silica sand and sepiolite respectively, the defluidization time decreased. The effect of the agglomerates break down because of the higher air excess was not enough to equilibrate the adhesion of the particles with the melting ash. When using silica sand, this reduction was very sharp. However, in case of sepiolite, the decrease was softer and, therefore, if the air excess ration is high enough there is some flexibility to select the fluidization flow rate without affect too much the defluidization time.

3.5. Agglomeration analysis

After each gasification experiment the particle size distribution of the bed material was measured. Different types of agglomerates were formed during the experiments as it can be seen in Fig. 8. Flat plate shape agglomerates on the bed surface appeared with silica sand for air excesses, u/u_{mf}, higher than 4. For lower gas velocities this agglomerate was less compact breaking into small pieces of particle aggregates. In silica sand tests, pellets floated on the bed surface creating the agglomerate in this part of the bed instead of inside the bed. However, when sepiolite was used, a completely different behavior was observed. The whole bed tended to agglomerate forming one big cylindrical shape. A better mixing between biomass pellets and bed material was observed during sepiolite experiments, leading to a better distribution of the elements that induce the agglomeration inside the bed. As a result, more homogenous agglomeration was obtained (Fig. 8).

Fig. 8. Agglomeration for silica sand and sepiolite for all air excesses.

The material that remained in the reactor after each gasification experiment was sieved. Fig.9 shows the size distribution of the bed material, where the ratio between the mass fraction of each sieve and the initial bed mass is shown. Notice that the initial mass fraction ratio is also represented (fresh bed material). The superficial gas velocity had an important effect on the size distribution of bed material. At higher air excesses more differences appeared between the original and final bed material distribution as it is shown in Fig. 9.

Fig. 9. Bed material distribution: a) silica sand and b) sepiolite.

In silica sand experiments, the bed material size distribution after the experiments is quite similar to the initial distribution (d_p = 425-600 μm) for low air excesses while a reduction of mass of this size around 50% was obtained in the case of u/u_{mf} = 10, most of it moving to the 600-850 μm sieve. In case of sepiolite, this reduction was achieved at lower u/u_{mf} ratios. Bigger agglomerates were formed for sepiolite than for silica sand at all air excess ratios. This effect is explained because when using silica sand, a flat plate shape was formed on the bed surface avoiding that the bed material which is beneath the agglomerate was affected by the agglomeration process. Furthermore, sepiolite experiments were longer than silica sand increasing the ash accumulation within the bed compared with silica sand experiments.

The ash accumulated in the bed when defluidization occurred was also calculated for the different u/u_{mf} ratios for silica sand and sepiolite. This variable is presented in Fig. 10 as the ratio of mass of ash accumulated in the bed at the onset of defluidization to mass of bed material in order to compare the two bed materials. Because the experimental facility did not have a system to collect flying ash and elutriated bed material, the amount of ash accumulated in the bed was obtained theoretically from the biomass ash content (Table 1) and the feeding rate of biomass (Table 3).

Fig. 10. Ash-to-bed mass ratio at the onset of defluidization: a) silica sand and b) sepiolite.

The ash accumulation phenomenon in the reactor during the gasification process was directly related with the u/u_{mf} ratio. Since the ER was kept at a constant value of 0.3 for all the experiments, an increase of the u/u_{mf} ratio entailed an increase of the feeding rate of biomass. However, for the sand at a ratio $u/u_{mf} = 10$, even if the biomass feeding rate was higher than for the $u/u_{mf}=6$ and $u/u_{mf}=8$ cases the low duration of the experiment, that is, the low defluidization time (Fig. 7), resulted in a lower amount of ash accumulated at the end of the experiment. On the other hand, for the sepiolite, the amount of ash accumulated in the reactor always increased with the u/u_{mf} ratio, as the decrease of the defluidization time with u/u_{mf} (Fig. 7) had a lower effect than the increase of the feeding rate of biomass.

Fig. 11 shows the mean bed temperature within the bed during the gasification process for each experiment. As it can be observed, for the sepiolite, when the ratio u/u_{mf} reached a value of 6 the bed temperature seemed to become independent of u/u_{mf}. This behavior means that the same fraction of biomass was transformed within the reactor. The vigorous fluidization in combination with the low ratio of sepiolite to biomass density promoted a high level of mixing in the reactor maintaining a constant and uniform bed temperature. In this case, the mixing time was lower than the reaction time.

Fig. 11. Mean bed temperature during the gasification experiment at different u/u_{mf} ratios for sand and sepiolite.

On the other hand, for silica sand, Fig. 11 shows that the mean bed temperature always increased with u/u_{mf}. This effect was directly related with the fraction of biomass transformed during the experiment. As u/u_{mf} increased, the fraction of biomass transformed increased and, consequently, the bed temperature rose. This effect can be explained by the enhance biomass mixing promoted by the augmented gas flow rate. The high density of the sand, made the biomass float at the top of the bed, and only increasing the flow rate the mixing level improved leading to higher fraction of biomass converted and higher bed temperatures. In this case the conversion was limited by the mixing time.

4. Conclusions

This work presents results on the defluidization time and agglomeration behavior of *Cynara Cardunculus* L. gasification in a BFB reactor using sepiolite as an alternative bed material.

Sepiolite increases considerably the defluidization time respect to silica sand. The lower density of sepiolite improved fuel mixing, leading into a better distribution of biomass and ash within the bed and avoiding hot zones.

The effect of air excess was studied for silica sand and sepiolite. An optimum value for u/u_{mf} ratio was obtained for silica sand ($u/u_{mf}=6$) and for sepiolite ($u/u_{mf}=4$), existing some flexibility to chose the u/u_{mf} ratio in the last case if this ratio is high enough.

The ash-to-bed mass ratio was also analyzed leading into a higher ash accumulation within the bed for the case of sepiolite. This ratio increased with u/u_{mf} but in a smaller way than the ash feeding rate. A constant fraction of biomass was transformed for sepiolite when u/u_{mf} ratio was higher than 6, being the mixing time lower than the reaction time. Contrary to this, the fraction of biomass transformed in silica sand experiments increased with u/u_{mf}, leading into a mixing time higher than the reaction time.

Different types of agglomerates were formed for silica sand and sepiolite. Flat plate shape agglomerates located at the top of the bed appeared during silica sand tests, contrary to sepiolite where the whole bed tended to agglomerate in one big cylindrical shape.

Time and frequency domain methods based on pressure fluctuations were used to determine the defluidization time. A good agreement was showed between them in accordance also with visual observations. Furthermore, the pressure signals measured in the plenum did not show significant differences between fluidization and defluidization in case of sepiolite and therefore, this location is not a good option to detect changes inside the bed when sepiolite is used as bed material.

Sepiolite has demonstrated its benefits in biomass gasification in advance of silica sand. Future works should validate the performance of sepiolite in terms of gas composition and tar generation comparing the catalytic effects, if any, with other bed materials.

Abbreviations

BFB Bubbling fluidized bed.

ER Equivalent ratio.

FB Fluidized bed.

MSW Municipal solid waste.

PSD Power spectral density.

References

[1] P. Basu, Biomass Gasification and Pyrolysis: Practical Design and Theory, Elsevier Inc., 2010.

[2] L. Devi, K.J. Ptasinski, F.J.J.G. Janssen, A review of the primary measures for tar elimination in biomass gasification processes, Biomass and Bioenergy. 24 (2003) 125–140.

[3] G. Xue, M. Kwapinska, A. Horvat, Z. Li, S. Dooley, W. Kwapinski, et al., Gasification of Miscanthus x giganteus in an Air-Blown Bubbling Fluidized Bed: A Preliminary Study of Performance and Agglomeration, Energy & Fuels. 28 (2014) 1121–1131.

[4] J. Zhou, Q. Chen, H. Zhao, X. Cao, Q. Mei, Z. Luo, et al., Biomass-oxygen gasification in a high-temperature entrained-flow gasifier., Biotechnol. Adv. 27 (2009) 606–11.

[5] D. Kunii, O. Levenspiel, Fluidization Engineering, 2nd ed., Butterworth-Heinemann, 1991.

[6] R. Warnecke, Gasification of biomass: comparison of fixed bed and fluidized bed gasifier, Biomass and Bioenergy. 18 (2000) 489–497.

[7] M. Bartels, W. Lin, J. Nijenhuis, F. Kapteijn, J.R. van Ommen, Agglomeration in fluidized beds at high temperatures: Mechanisms, detection and prevention, Prog. Energy Combust. Sci. 34 (2008) 633–666.

[8] A.A. Khan, W. de Jong, P.J. Jansens, H. Spliethoff, Biomass combustion in fluidized bed boilers: Potential problems and remedies, Fuel Process. Technol. 90 (2009) 21–50.

[9] W. Lin, K. Dam-Johansen, F. Frandsen, Agglomeration in bio-fuel fired fluidized bed combustors, Chem. Eng. J. 96 (2003) 171–185.

[10] T. Liliedahl, K. Sjöström, K. Engvall, C. Rosén, Defluidisation of fluidised beds during gasification of biomass, Biomass and Bioenergy. 35 (2011) S63–S70.

[11] C. Sevonius, P. Yrjas, M. Hupa, Defluidization of a quartz bed – Laboratory experiments with potassium salts, Fuel. 127 (2013) 161–168.

[12] J. Werther, M. Saenger, E.-U. Hartge, T. Ogada, Z. Siagi, Combustion of agricultural residues, Prog. Energy Combust. Sci. 26 (2000) 1–27.

[13] L.E. Fryda, K.D. Panopoulos, E. Kakaras, Agglomeration in fluidised bed gasification of biomass, Powder Technol. 181 (2008) 307–320.

[14] M. Siedlecki, W. de Jong, Biomass gasification as the first hot step in clean syngas production process – gas quality optimization and primary tar reduction measures in a 100 kW thermal input steam–oxygen blown CFB gasifier, Biomass and Bioenergy. 35 (2011) S40–S62.

[15] R. Giustetto, O. Wahyudi, I. Corazzari, F. Turci, Chemical stability and dehydration behavior of a sepiolite/indigo Maya Blue pigment, Appl. Clay Sci. 52 (2011) 41–50.

[16] H.H. Murray, M. Pozo, E. Galán, An Introduction to Palygorskite and Sepiolite Deposits — Location , Geology and Uses, in: E. Galán, A. Singer (Eds.), Dev. Palygorskite-Sepiolite Res., Elsevier, Amsterdam, 2011: pp. 85–99.

[17] J. Ruud van Ommen, R.-J. de Korte, C.M. van den Bleek, Rapid detection of defluidization using the standard deviation of pressure fluctuations, Chem. Eng. Process. Process Intensif. 43 (2004) 1329–1335.

[18] R. Chirone, F. Miccio, F. Scala, Mechanism and prediction of bed agglomeration during fluidized bed combustion of a biomass fuel: Effect of the reactor scale, Chem. Eng. J. 123 (2006) 71–80.

[19] F. Scala, R. Chirone, Characterization and Early Detection of Bed Agglomeration during the Fluidized Bed Combustion of Olive Husk, Energy & Fuels. 20 (2006) 120–132.

[20] J. Gómez-Hernández, A. Soria-Verdugo, J.V. Briongos, D. Santana, Fluidized bed with a rotating distributor operated under defluidization conditions, Chem. Eng. J. 195-196 (2012) 198–207.

[21] P. Abelha, C. Franco, F. Pinto, H. Lopes, I. Gulyurtlu, J. Gominho, et al., Thermal Conversion of Cynara cardunculus L . and Mixtures with Eucalyptus globulus by Fluidized-Bed Combustion and Gasification, Energy & Fuels. 27 (2013) 6725–6737.

[22] J. Fernández, M.D. Curt, State of the art of Cynara Cardunculus L. as an energy crop, in: L. Sjunnesson, J.E. Carrasco, P. Helm, A. Grassi (Eds.), 14th Eur. Conf. Technol. Exhib. Biomass Energy, Ind. Clim. Prot., ETA-Renewable Energies and WIP Renewable Energies, Paris, 2005: pp. 22–27.

[23] A. Ierna, G. Mauromicale, Cynara cardunculus L. genotypes as a crop for energy purposes in a Mediterranean environment, Biomass and Bioenergy. 34 (2010) 754–760.

[24] P. Grammelis, A. Malliopoulou, P. Basinas, N.G. Danalatos, Cultivation and characterization of Cynara Cardunculus for solid biofuels production in the Mediterranean region, Int. J. Mol. Sci. 9 (2008) 1241–58.

[25] J. Gominho, a. Lourenço, P. Palma, M.E. Lourenço, M.D. Curt, J. Fernández, et al., Large scale cultivation of Cynara cardunculus L. for biomass production—A case study, Ind. Crops Prod. 33 (2011) 1–6.

[26] L.G. Angelini, L. Ceccarini, N. Nassi o Di Nasso, E. Bonari, Long-term evaluation of biomass production and quality of two cardoon (Cynara cardunculus L.) cultivars for energy use, Biomass and Bioenergy. 33 (2009) 810–816.

[27] E.G. Papazoglou, S. Rozakis, Cardoon cultivation for combined bioenergy production and cadmium phytoextraction : an economic evaluation, in: Proc. 3rd Int. CEMEPE SECOTOX Conf., 2011: pp. 637–642.

[28] J.M. Encinar, J.F. González, J. González, Fixed-bed pyrolysis of Cynara cardunculus L . Product yields and compositions, Fuel. 68 (2000) 209–222.

[29] J.M. Encinar, J.F. González, J. González, Steam gasification of Cynara cardunculus L .: influence of variables, Fuel Process. Technol. 75 (2002) 27–43.

[30] C. Christodoulou, C. Tsekos, G. Tsalidis, M. Fantini, K.D. Panopoulos, W. de Jong, et al., Attempts on cardoon gasification in two different Circulating fluidized Beds, Case Stud. Therm. Eng. 4 (2014) 42–52.

[31] V. Skoulou, G. Koufodimos, Z. Samaras, a Zabaniotou, Low temperature gasification of olive kernels in a 5-kW fluidized bed reactor for H2-rich producer gas, Int. J. Hydrogen Energy. 33 (2008) 6515–6524.

[32] C. Pecharromán, A. Esteban-Cubillo, I. Montero, J.S. Moya, E. Aguilar, J. Santarén, et al., Monodisperse and Corrosion-Resistant Metallic Nanoparticles Embedded into Sepiolite Particles for Optical and Magnetic Applications, J. Am. Ceram. Soc. 89 (2006) 3043–3049.

[33] M. Doğan, Y. Özdemir, M. Alkan, Adsorption kinetics and mechanism of cationic methyl violet and methylene blue dyes onto sepiolite, Dye. Pigment. 75 (2007) 701–713.

[34] D. Zadaka-Amir, N. Bleiman, Y.G. Mishael, Sepiolite as an effective natural porous adsorbent for surface oil-spill, Microporous Mesoporous Mater. 169 (2013) 153–159.

[35] D. Geldart, Types of Gas Fluidization, Powder. 7 (1973) 285–292.

[36] S. Sasic, B. Leckner, F. Johnsson, Fluctuations and waves in fluidized bed systems: The influence of the air-supply system, Powder Technol. 153 (2005) 176–195.

[37] A. Gómez-Barea, R. Arjona, P. Ollero, Pilot-Plant Gasification of Olive Stone: a Technical Assessment, Energy & Fuels. 19 (2005) 598–605.

[38] Z.A.B.Z. Alauddin, P. Lahijani, M. Mohammadi, A.R. Mohamed, Gasification of lignocellulosic biomass in fluidized beds for renewable energy development: A review, Renew. Sustain. Energy Rev. 14 (2010) 2852–2862.

[39] M. Puncochár, J. Drahos, J. Cermák, K. Selucký, Evaluation of minimum fluidizing velocity gas fluidized bed from pressure fluctuations, Chem. Eng. Commun. 35 (1985) 81–87.

[40] J. Ruud van Ommen, S. Sasic, J. van der Schaaf, S. Gheorghiu, F. Johnsson, M.-O. Coppens, Time-series analysis of pressure fluctuations in gas–solid fluidized beds – A review, Int. J. Multiph. Flow. 37 (2011) 403–428.

[41] P. Welch, The use of fast Fourier transform for the estimation of power spectra: a method based on time averaging over short, modified periodograms, IEEE Trans. Audio Electroacust. 15 (1967) 70–73.

[42] F. Johnsson, R.C. Zijerveld, J.C. Schouten, C.M. van den Bleek, Characterization of fluidization regimes by time-series analysis of pressure fluctuations, Int. J. Multiph. Flow. 26 (2000) 663–715.

[43] M. Fiorentino, A. Marzocchella, P. Salatino, Segregation of fuel particles and volatile matter during devolatilization in a fluidized bed reactor II. Experimental, Chem. Eng. Sci. 52 (1997) 1909–1922.

[44] M. Fiorentino, A. Marzocchella, P. Salatino, Segregation of fuel particles and volatile matter during devolatilization in a fluidized bed reactor I. Model development, Chem. Eng. Sci. 52 (1997) 1893–1908.

[45] Q. Guo, G. Yue, T. Suda, J. Sato, Flow characteristics in a bubbling fluidized bed at elevated temperature, Chem. Eng. Process. 42 (2003) 439–447.

[46] S.C. Saxena, N.S. Rao, S.J. Zhou, Fluidization characteristics of gas fluidized beds at elevated temperatures, Energy. 15 (1990) 1001–1014.

[47] S.C. Saxena, N.S. Rao, V.N. Tanjore, Diagnostic Procedures for Establishing the Quality of Fluidization of Gas-Solid Systems, Exp. Therm. Fluid Sci. 6 (1993) 56–73.

[48] H.T. Bi, A critical review of the complex pressure fluctuation phenomenon in gas–solids fluidized beds, Chem. Eng. Sci. 62 (2007) 3473–3493.

[49] C.-L. Lin, J.-H. Kuo, M.-Y. Wey, S.-H. Chang, K.-S. Wang, Inhibition and promotion: The effect of earth alkali metals and operating temperature on particle agglomeration/defluidization during incineration in fluidized bed, Powder Technol. 189 (2009) 57–63.

Figure captions

Fig 1. Experimental facility.

Fig 2. Snapshots (using the quartz reactor) obtained during gasification experiments ($u/u_{mf} = 4$): a), b) and c) silica sand; d), e) and f) sepiolite.

Fig. 3. Pressure and temperature signals for silica sand and sepiolite ($u/u_{mf} = 4$): a) and d) pressure fluctuations inside the bed; b) and e) pressure drop across the bed; c) and f) relative temperature difference between different heights.

Fig. 4. Standard deviation of pressure fluctuations inside the bed: a) silica sand and b) sepiolite.

Fig. 5. PSD of pressure fluctuations for sepiolite ($u/u_{mf}=6$) at two different instants. At a time of 41 min the bed was fluidized and at a time of 45 min the bed was defluidized. The dominant frequency of each spectrum is marked with a circle in the plot.

Fig. 6. Dominant frequency of the power spectrum of pressure fluctuations inside the bed as a function of time: a) silica sand and b) sepiolite.

Fig. 7. Defluidization time: a) silica sand and b) sepiolite.

Fig. 8. Agglomeration for silica sand and sepiolite for all air excesses.

Fig. 9. Bed material distribution: a) silica sand and b) sepiolite.

Fig. 10. Ash-to-bed mass ratio at the onset of defluidization: a) silica sand and b) sepiolite.

Fig. 11. Mean bed temperature during the gasification experiment at different u/u_{mf} ratios for sand and sepiolite.

Figure1

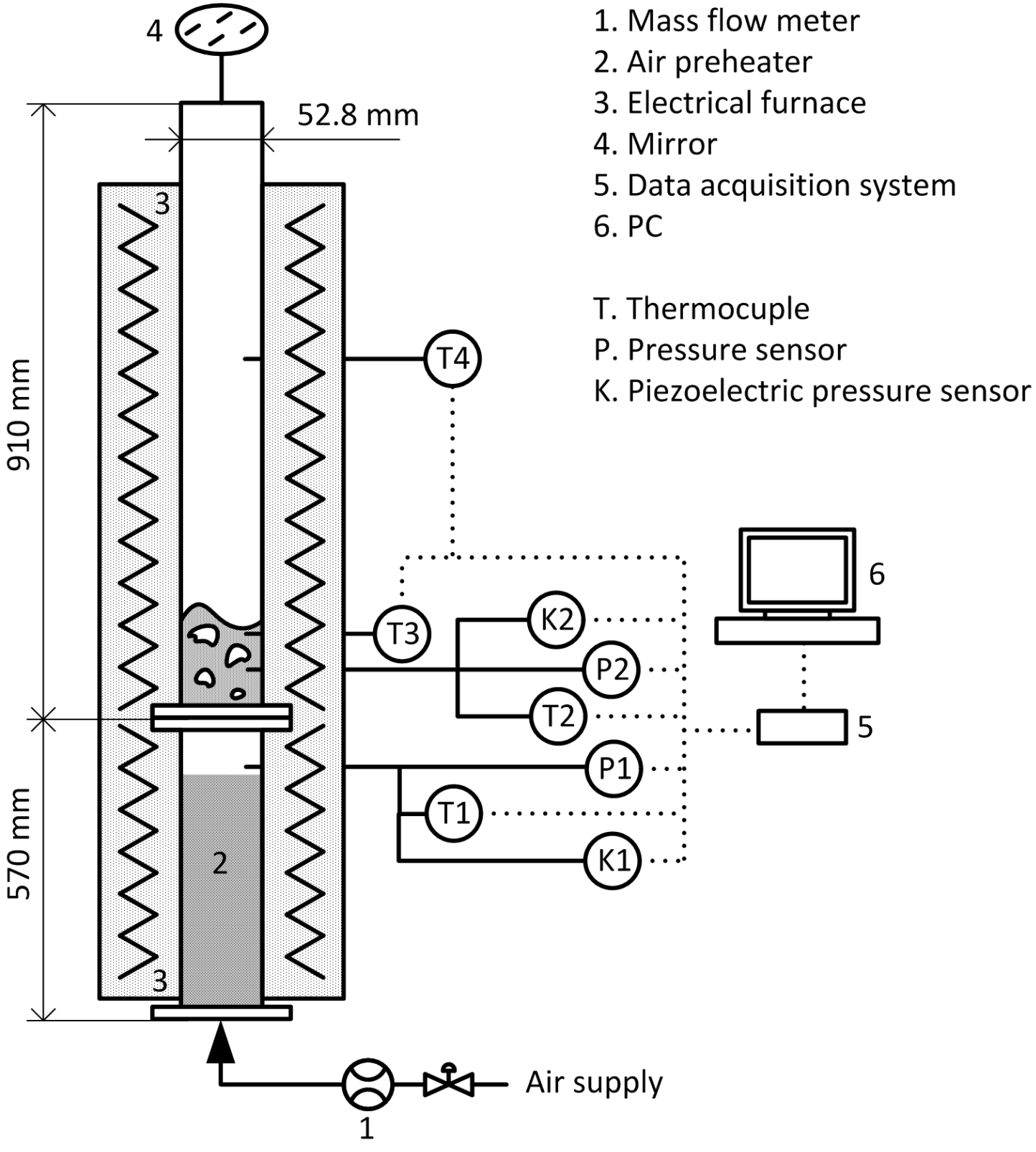
1. Mass flow meter
2. Air preheater
3. Electrical furnace
4. Mirror
5. Data acquisition system
6. PC
T. Thermocuple
P. Pressure sensor
K. Piezoelectric pressure sensor
4
52.8 mm
3
910 mm
T4
T3
K2
P2
T2
P1
T1
K1
6
5
570 mm
2
3
Air supply
1

Figure2

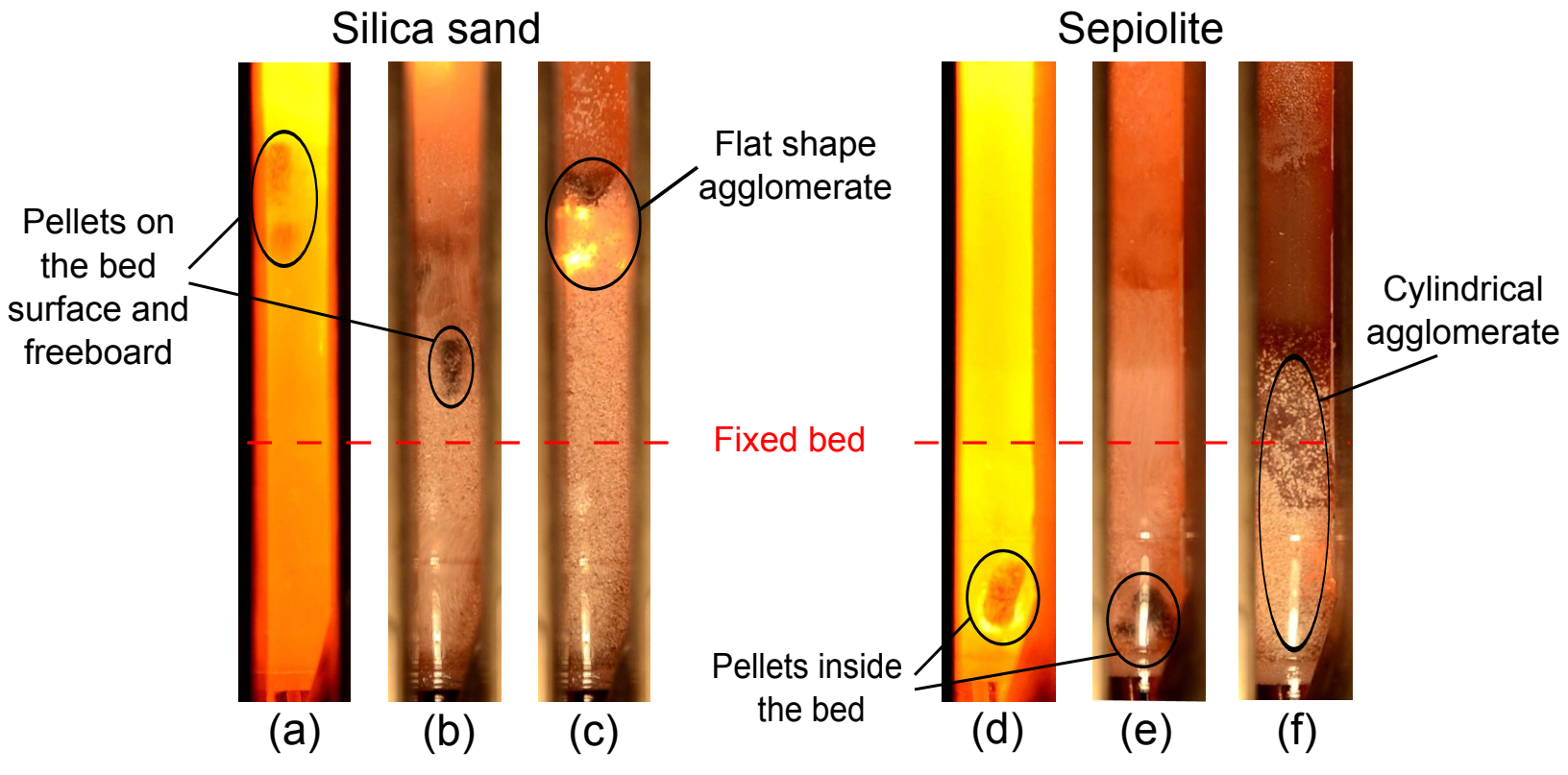
Silica sand
Sepiolite
Flat shape agglomerate
Pellets on the bed surface and freeboard
Cylindrical agglomerate
Fixed bed
Pellets inside the bed
(a)
(b)
(c)
(d)
(e)
(f)

Figure3

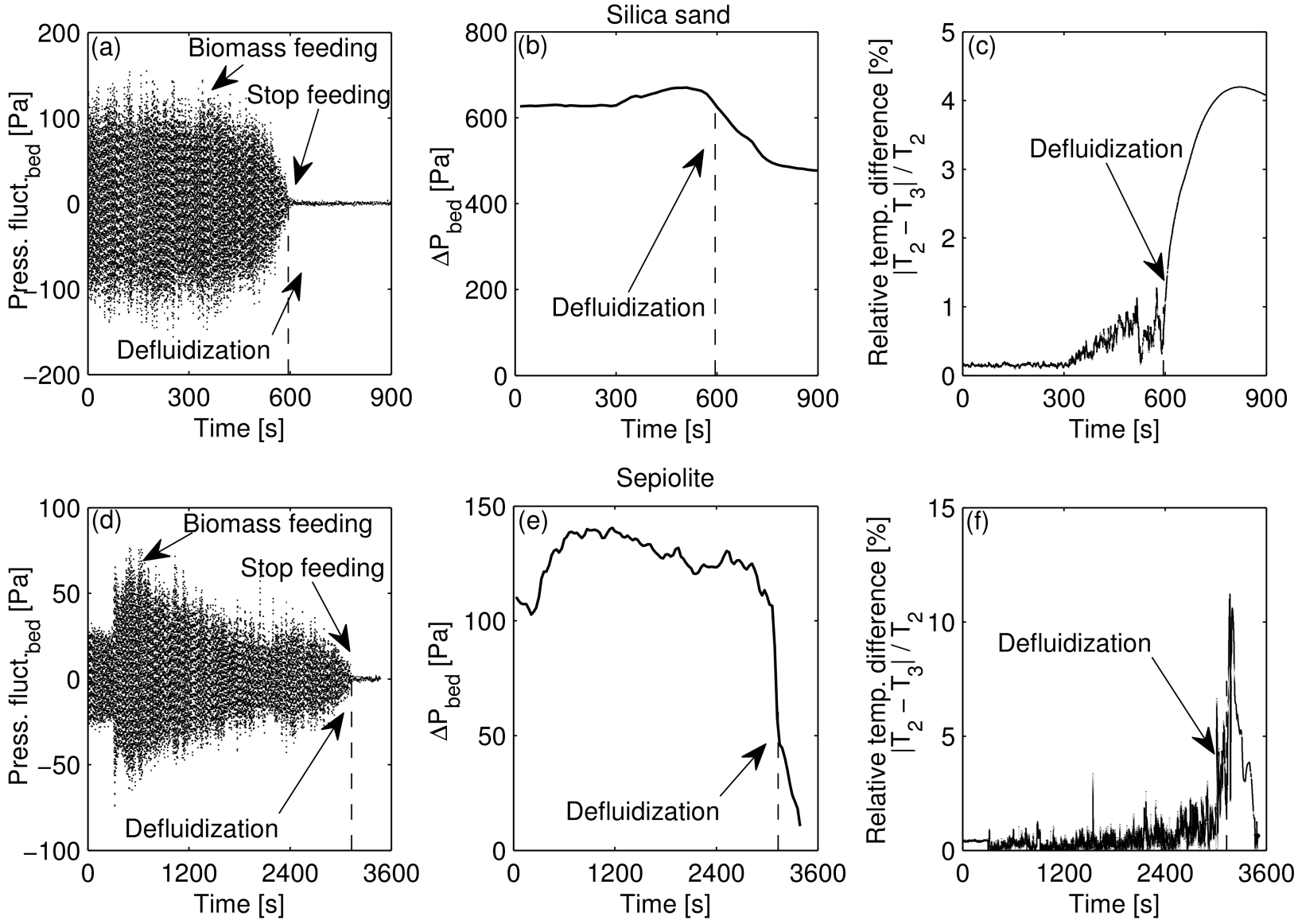
Silica sand
(a)
Biomass feeding
Stop feeding
Defluidization
Press. fluct$_{bed}$ [Pa]
Time [s]
(b)
Defluidization
ΔP_{bed} [Pa]
Time [s]
(c)
Defluidization
Relative temp. difference $|T_2 - T_3| / T_2$
Time [s]
Sepiolite
(d)
Biomass feeding
Stop feeding
Defluidization
Press. fluct$_{bed}$ [Pa]
Time [s]
(e)
Defluidization
ΔP_{bed} [Pa]
Time [s]
(f)
Defluidization
Relative temp. difference $|T_2 - T_3| / T_2$
Time [s]

Figure4

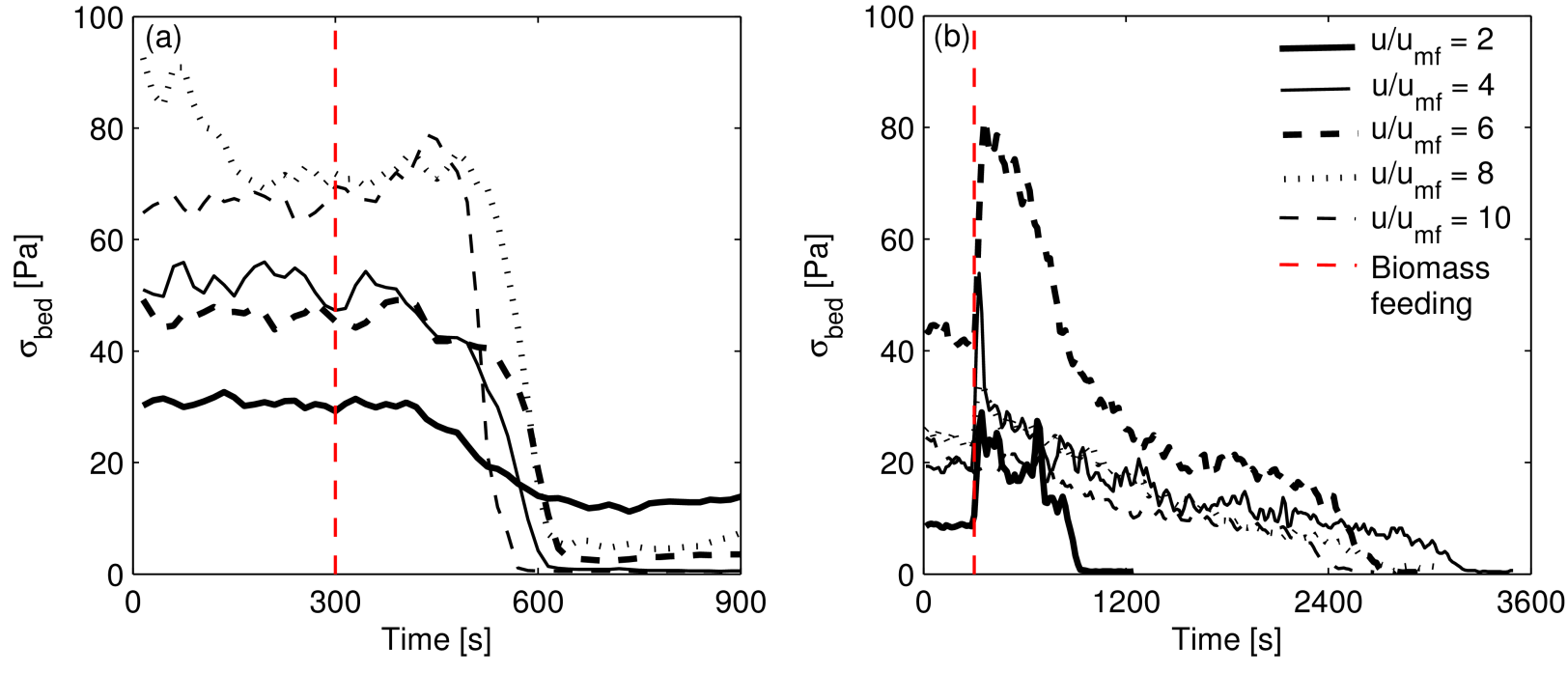
(a)
(b)
100
80
60
40
20
0
σbed [Pa]
0
300
600
900
1200
2400
3600
Time [s]
u/umf = 2
u/umf = 4
u/umf = 6
u/umf = 8
u/umf = 10
Biomass feeding

Figure5

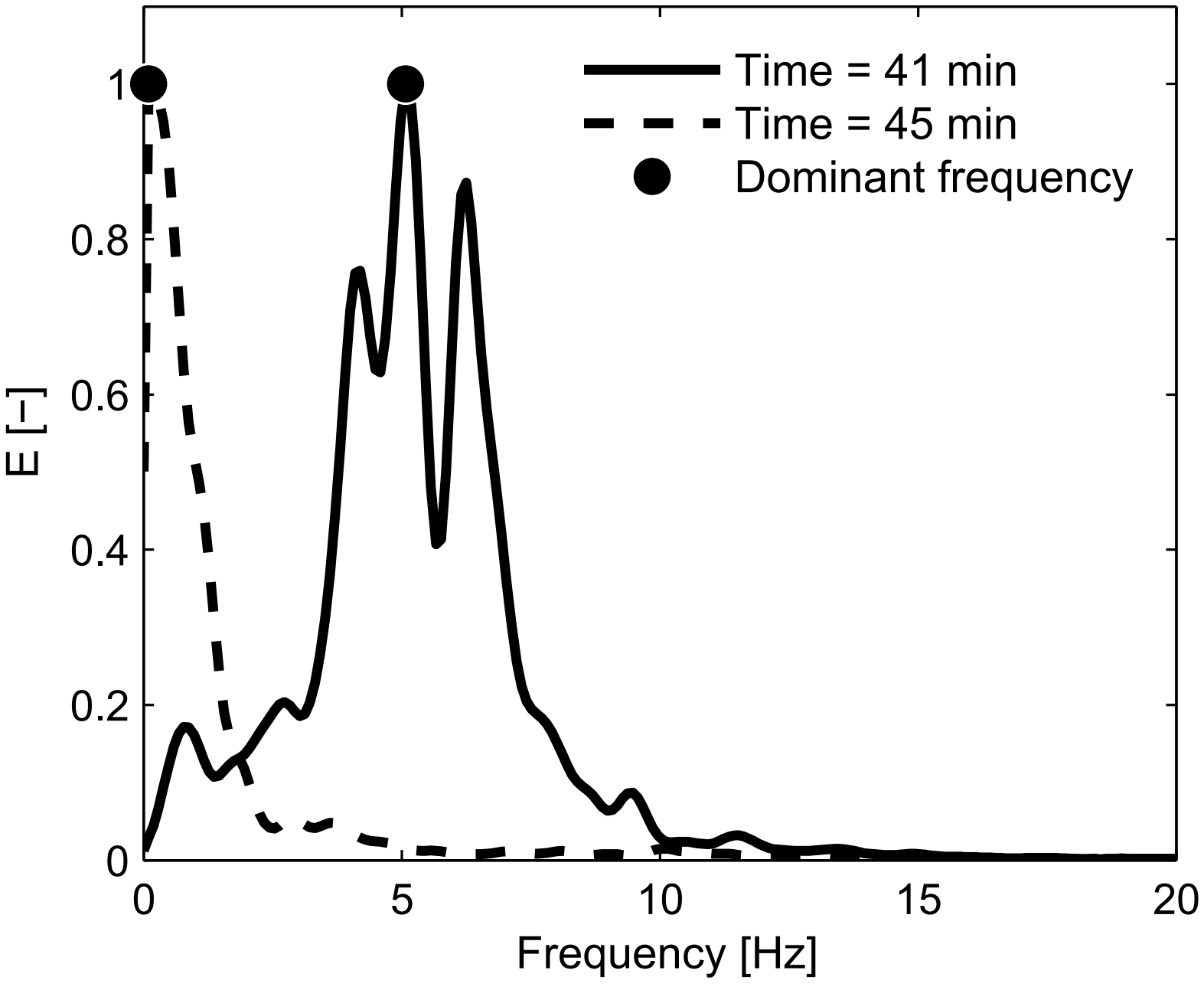
Time = 41 min
Time = 45 min
Dominant frequency
E [-]
Frequency [Hz]
0
0.2
0.4
0.6
0.8
1
0
5
10
15
20

Figure6

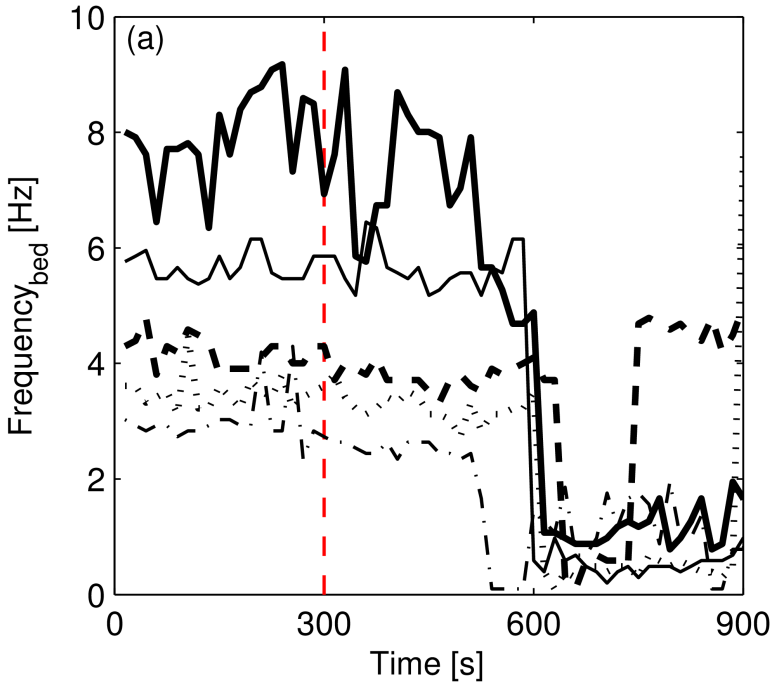
(a)
Frequency$_{bed}$ [Hz]
Time [s]
0
2
4
6
8
10
0
300
600
900

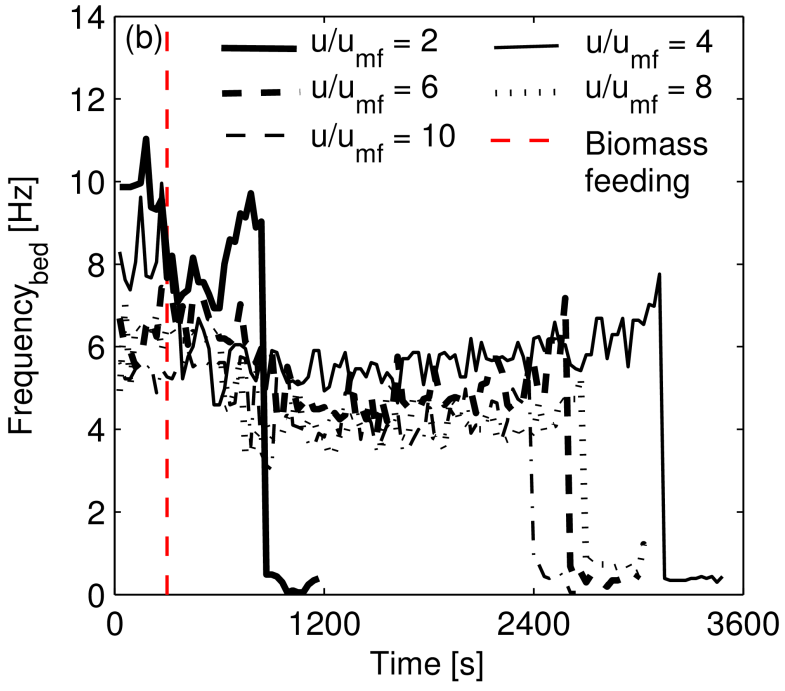
(b)
u/u$_{mf}$ = 2
u/u$_{mf}$ = 4
u/u$_{mf}$ = 6
u/u$_{mf}$ = 8
u/u$_{mf}$ = 10
Biomass feeding
Frequency$_{bed}$ [Hz]
Time [s]
0
2
4
6
8
10
12
14
0
1200
2400
3600

Figure7

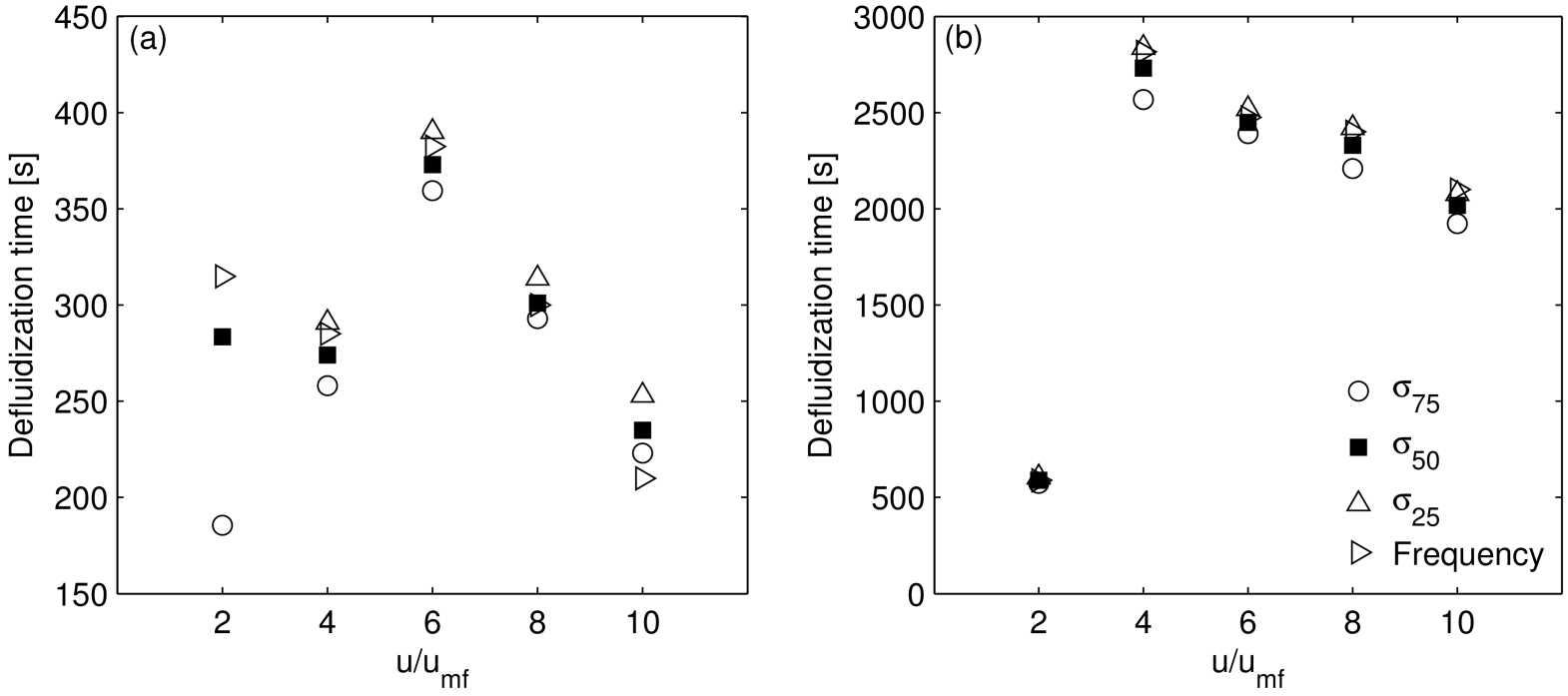
(a)
Defluidization time [s]
450
400
350
300
250
200
150
2
4
6
8
10
u/u_mf
(b)
Defluidization time [s]
3000
2500
2000
1500
1000
500
0
2
4
6
8
10
u/u_mf
σ75
σ50
σ25
Frequency

Figure8

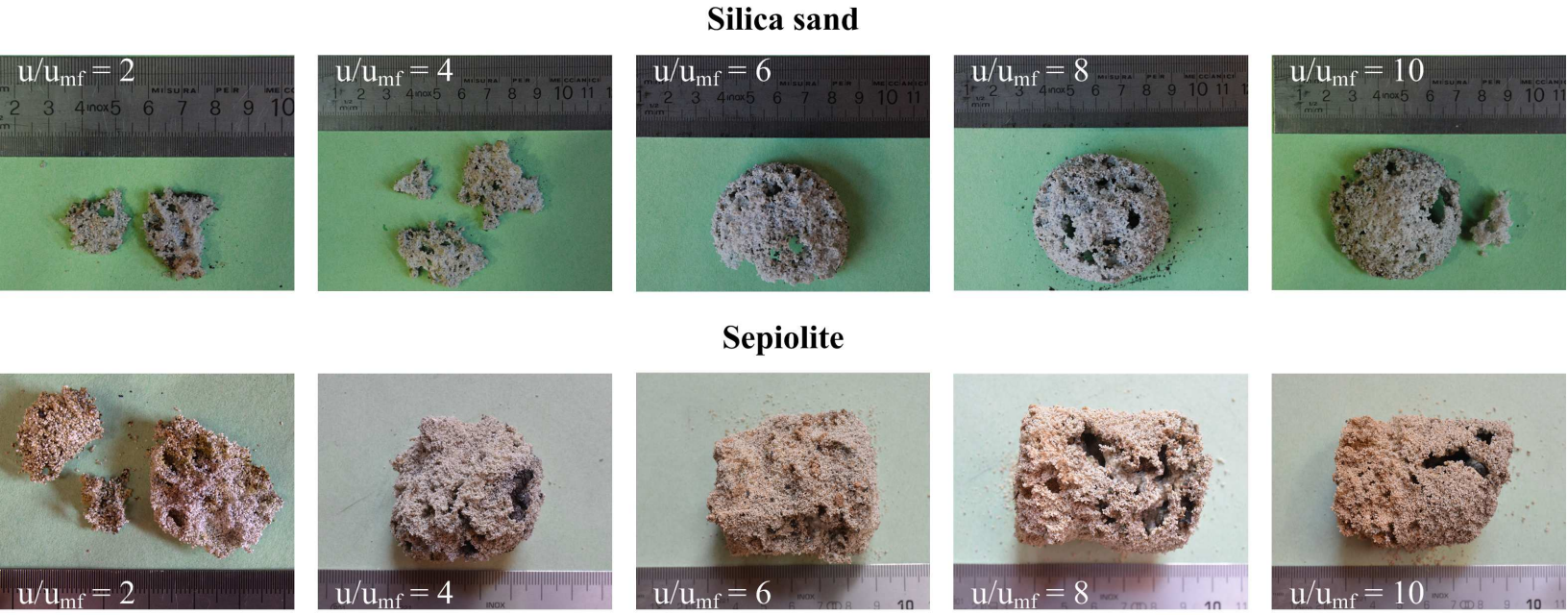
Silica sand
u/u$_{mf}$ = 2
u/u$_{mf}$ = 4
u/u$_{mf}$ = 6
u/u$_{mf}$ = 8
u/u$_{mf}$ = 10
Sepiolite
u/u$_{mf}$ = 2
u/u$_{mf}$ = 4
u/u$_{mf}$ = 6
u/u$_{mf}$ = 8
u/u$_{mf}$ = 10

Figure9

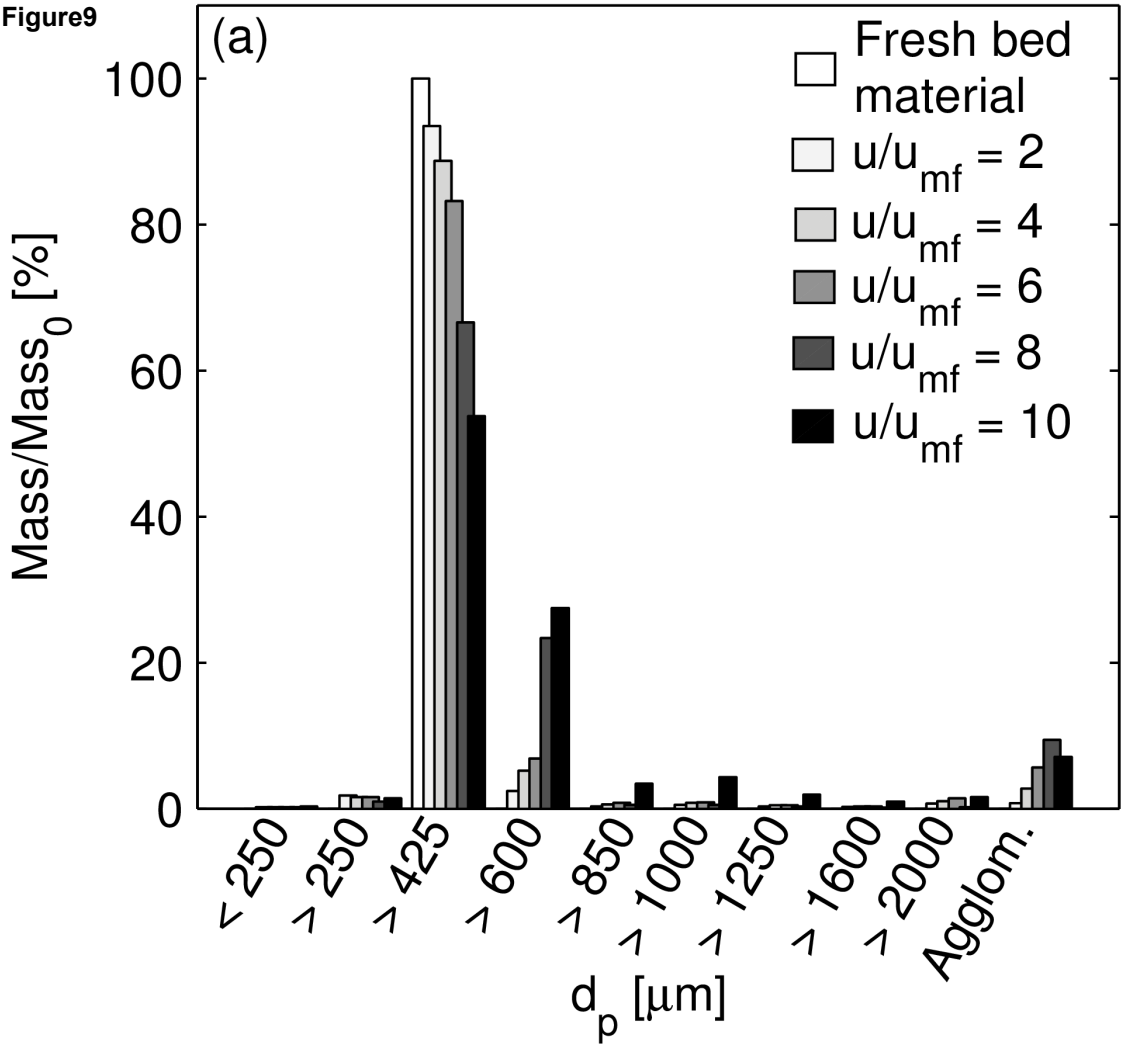
(a)
Fresh bed material
u/u_mf = 2
u/u_mf = 4
u/u_mf = 6
u/u_mf = 8
u/u_mf = 10
Mass/Mass_0 [%]
0
20
40
60
80
100
< 250
> 250
> 425
> 600
> 850
> 1000
> 1250
> 1600
> 2000
Agglom.
d_p [µm]

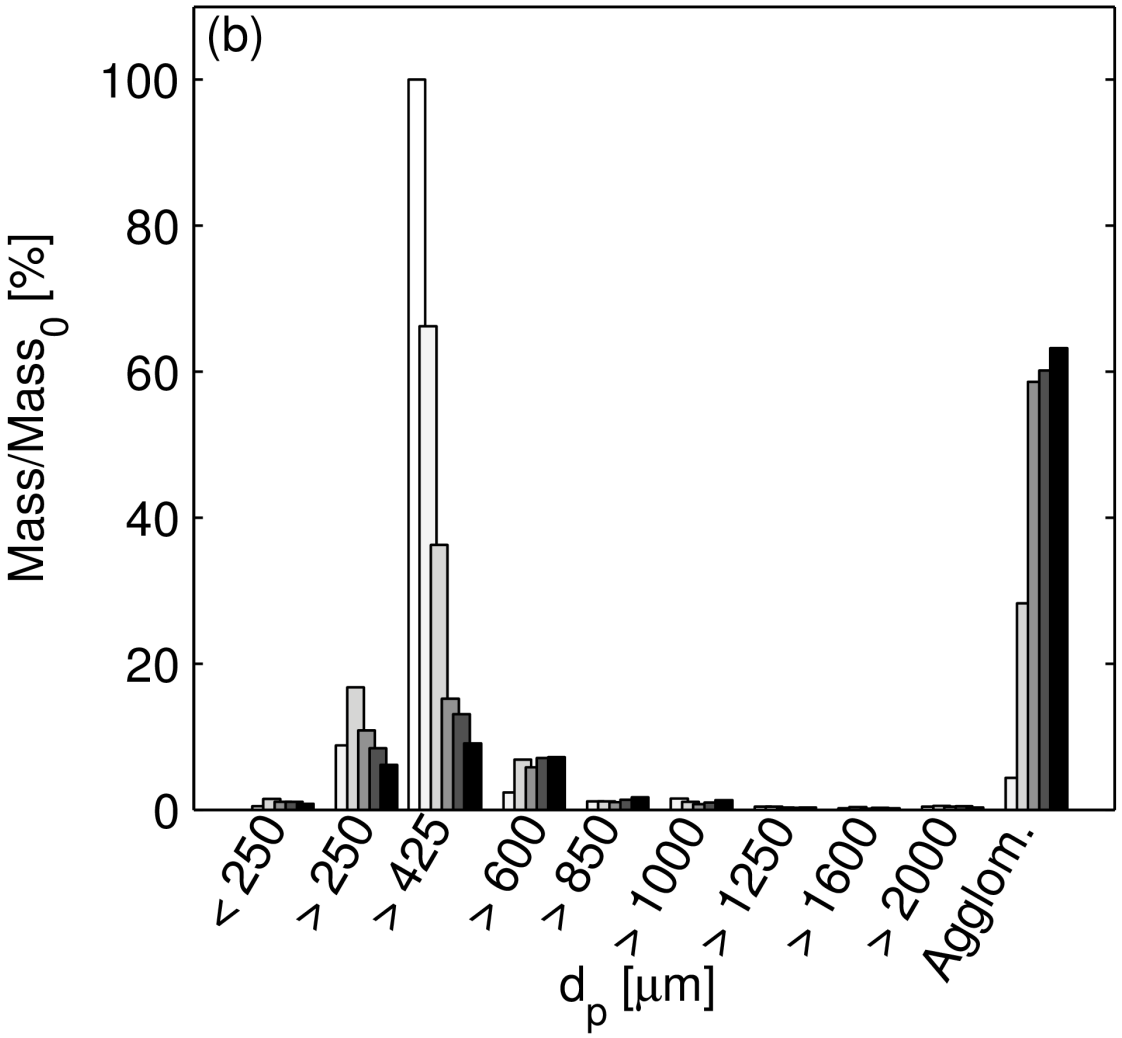
(b)
Mass/Mass_0 [%]
0
20
40
60
80
100
< 250
> 250
> 425
> 600
> 850
> 1000
> 1250
> 1600
> 2000
Agglom.
d_p [µm]

Figure10

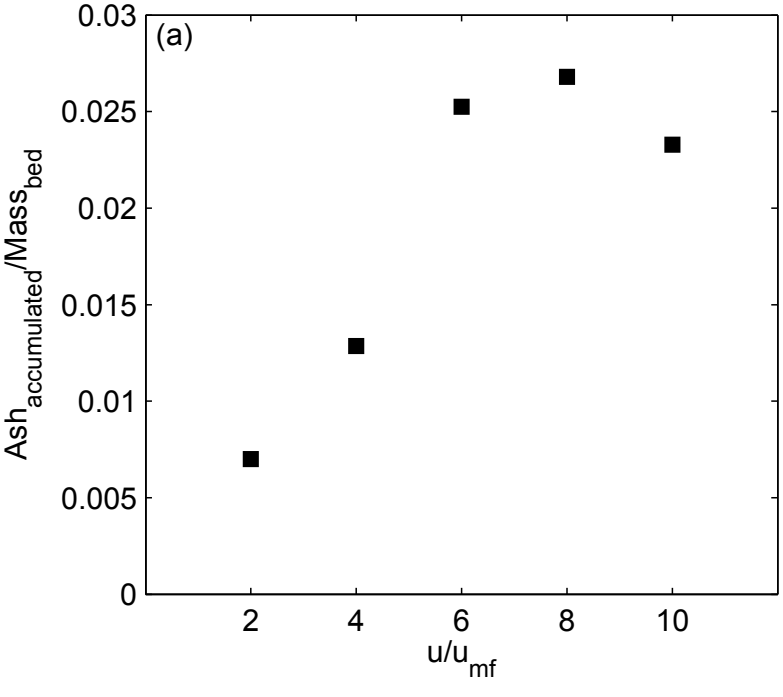
(a)
0.03
0.025
0.02
0.015
0.01
0.005
0
2
4
6
8
10
u/u_mf
Ash_accumulated/Mass_bed

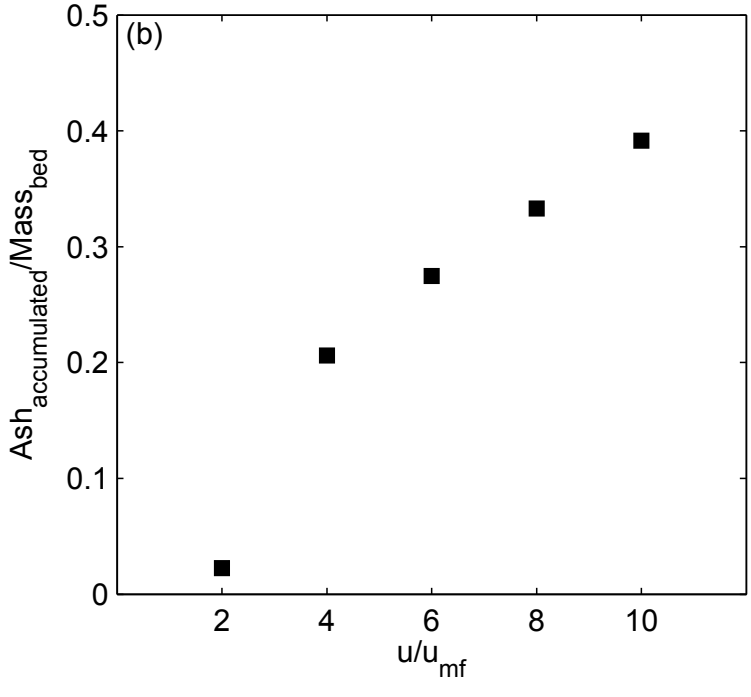
(b)
0.5
0.4
0.3
0.2
0.1
0
2
4
6
8
10
u/u_mf
Ash_accumulated/Mass_bed

Figure11

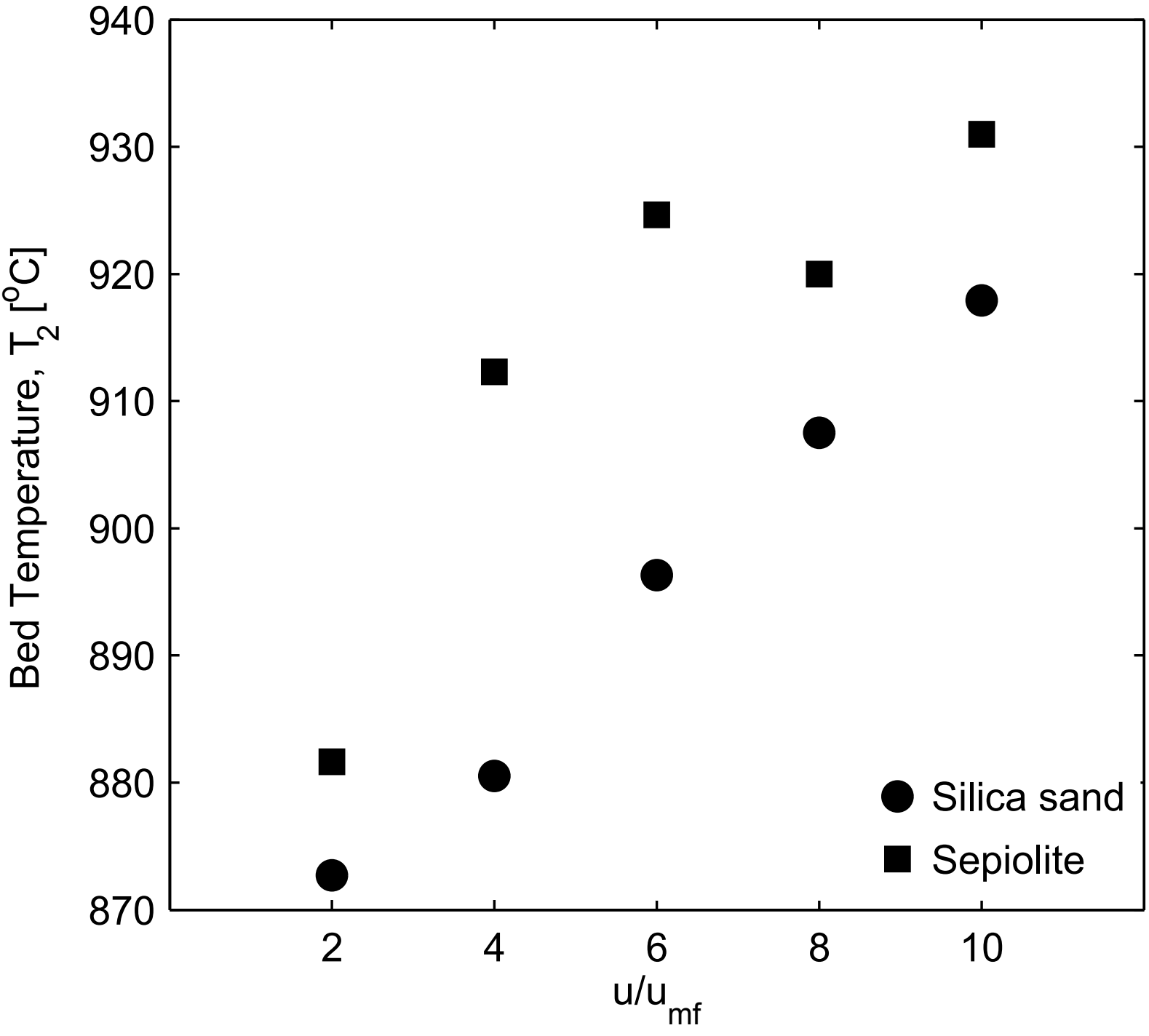
940
930
920
910
900
890
880
870
Bed Temperature, T_2 [^oC]
2
4
6
8
10
u/u_{mf}
Silica sand
Sepiolite